Structural Engineering and Mechanics, *Vol. 64, No. 4 (2017) 461-472*
DOI: https://doi.org/10.12989/sem.2017.64.4.461

Analysis on the dynamic characteristics of RAC frame structures

Changqing Wang[*1,2] and Jianzhuang Xiao[2a]

[1]*School of Mechanics and Civil Engineering, China University of Mining and Technology, Xuzhou 221116, China*
[2]*College of Civil Engineering, Tongji University, Shanghai 200092, China*

(Received August 3, 2016, Revised July 22, 2017, Accepted July 23, 2017)

Abstract. The dynamic tests of recycled aggregate concrete (RAC) are carried out, the rate-dependent mechanical models of RAC are proposed. The dynamic mechanical behaviors of RAC frame structure are investigated by adopting the numerical simulation method of the finite element. It is indicated that the lateral stiffness and the hysteresis loops of RAC frame structure obtained from the numerical simulation agree well with the test results, more so for the numerical simulation which is considered the strain rate effect than for the numerical simulation with strain rate excluded. The natural vibration frequency and the lateral stiffness increase with the increase of the strain rate. The dynamic model of the lateral stiffness is proposed, which is reasonably applied to describe the effect of the strain rate on the lateral stiffness of RAC frame structure. The effect of the strain rate on the structural deformation and capacity of RAC is analyzed. The analyses show that the inter-story drift decreases with the increase of the strain rate. However, with the increasing strain rate, the structural capacity increases. The dynamic models of the base shear coefficient and the overturning moment of RAC frame structure are developed. The dynamic models are important and can be used to evaluate the strength deterioration of RAC structure under dynamic loading.

Keywords: recycled aggregate concrete (RAC); dynamic characteristic; strain rate effect; natural frequency; lateral stiffness; hysteresis loops; inter-story drift; shear coefficient; overturning moment

1. Introduction

A great deal of research has been carried out to develop RAC worldwide. The material property of recycled aggregate (Wang *et al*. 2012, Cardoso *et al*. 2016, Behera *et al.* 2014, Ashtiani *et al.* 2014), the material mechanic performance of RAC (ACI Committee 555 2002, Lotfi *et al.* 2015, Zhang and Zong 2014), the constitutive relationship of stress-strain of RAC (Wang *et al.* 2014, Zhao *et al.* 2015), and the structural behaviors of RAC (Shi *et al.* 2015, Rahal and AI-Khaleefi 2015, Gnjatovic *et al.* 2013) are experimentally studied and theoretically analyzed. It has been found that there is a slight difference in mechanical properties between recycled aggregate concrete (RAC) and natural aggregate concrete (NAC). However, for RAC it is still sufficient for practical applications in civil engineering. This is further confirmed by recent experimental studies of the mechanical behavior of structural members made of RAC (Fathifazl *et al.* 2009, Wang 2012, Ajdukiewicz and Kliszczewicz 2007, Zhang *et al.* 2016). It may be noted that most of the above studies on RAC were carried out under static or quasi-static loading.

Concrete is a typical rate-dependent material, and the strength, the stiffness and the ductility (or brittleness) are significantly influenced by the loading rates. The strain rate at critical sections from the dynamic loads may be up to 1 /s for the reinforced concrete structure subjected to strong earthquake ground motion excitations (Bischoff and Perry 1991). The properties of structural materials at dynamic loading will be different from those at static loading (Wakabayashi *et al.* 1984, Shing and Mahin 1988). A few studies on the dynamic mechanical properties of RAC are investigated in recent years. Xiao *et al.* (2014) perform a series of experiments on modeled RAC at uniaxial compressive loading condition and observe the compressive strength and elastic modulus increase with the increase of strain rate. The split Hopkinson pressure bar tests of RAC at compression loading condition are carried out by Lu *et al.* (2014). Results show that impact properties of RAC exhibit strong strain rate dependency, and increase approximately linearly with strain rate. The compressive behavior of RAC with different recycled coarse aggregate (RCA) replacement percentages is experimentally investigated under quasi-static to high strain rate loading by Xiao *et al.* (2015), and the strain rate effects on the failure pattern, compressive strength, initial elastic modulus and peak strain are studied. The dynamic mechanical behaviors of RAC structures at high strain rate representative of seismic conditions were also investigated experimentally in recent years. Zhang *et al.* (2014) performed shaking table tests on four 1/5 scaled RAC frame-shear wall structures with concealed bracing detail. The dynamic characteristics, dynamic response and failure mode of each model were compared and analyzed. Shaking table tests on a full-scale model of RAC block masonry building with the tie column + ring beam + cast-in-place slab system was carried out by Wang and Xiao (2012a). The dynamic characteristics, the seismic performance, and the damage assessment of RAC frame structure were analyzed under different earthquake levels.

∗Corresponding author, Ph.D.
E-mail: changqingwang@tongji.edu.cn
[a]Ph.D.

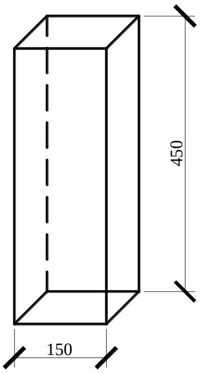

(a) Dimension of specimen (unit: mm)

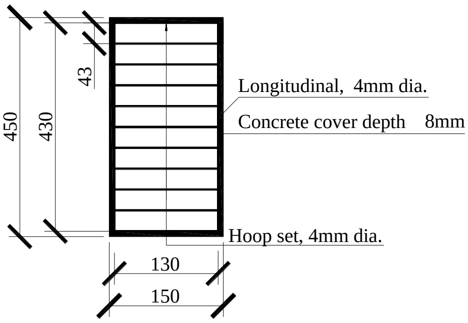

(b) Reinforcements (unit: mm)

Fig. 1 the test units

Fig. 2 Test setup

There is little evidence of numerical model with the inclusion of strain rate effect finding a place in the seismic analysis of framed structures made of recycled aggregate concrete. For the nonlinear analysis of reinforced concrete structures, a variety of models have been considered (CEB 1993, Penelis and Kappos 1997, Taucer *et al.* 1991, Tu and Lu 2011a, b, Kwak *et al*. 2004, Valipour and Foster 2010). These range from refined and complex local models to simplified global models. The present study concentrates on the discrete finite element models that within limits provide satisfactory response predictions with moderate numerical effort compared to refined finite element models and more realistic and useful than the simplified models (Zeris and Mahin 1991, Taucer *et al*. 1991, Shao *et al.* 2005). Therefore, the model is the best compromise between simplicity and accuracy in nonlinear seismic response studies and represents the simplest class of model that still allows significant insight into the seismic response of members and of the entire structure.

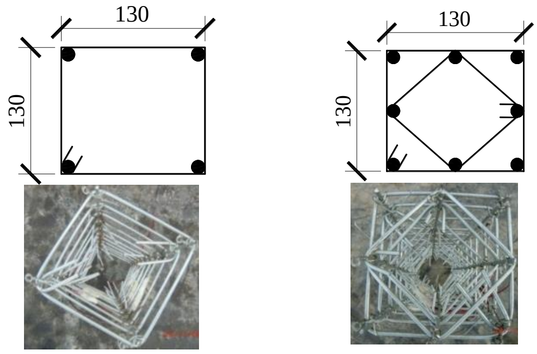

(a) A-CRAC (b) B-CRAC

Fig. 3 Arrangement of transverse hoops

In this study, the dynamic tests of recycled aggregate concrete (RAC) are carried out, the rate-dependent mechanical models of RAC are proposed. The dynamic mechanical behaviors of RAC frame structure are investigated by adopting the numerical simulation method of the finite element. The lateral stiffness and the hysteresis loops of RAC frame structure obtained from the numerical simulation are analyzed and compared with the shaking table test results.

2. Dynamic tests of RAC

2.1 Strain-rate-dependent model of concrete

To investigate the dynamic properties of RAC, nine unconfined recycled aggregate concrete (URAC) and eighteen confined recycled aggregate concrete (CRAC) test units with RCA replacement ratio of 100% were fabricated. The test units (shown in Fig. 1) have a section that is 150 mm square and 450 mm high. All dynamic tests were conducted in an **MTS 815** concrete testing system, which is an electro-hydraulic servo-controlled testing machine with a vertical load capacity of up to 2500 kN. The test set up is plotted in Fig. 2. Two arrangements of transverse hoop reinforcement representative of current practice were used as shown in Fig. 3. Herein, *A* stands for the type of square stirrups which is the typical arrangement for 4-bar column, and *B* stands for the type of overlapping stirrups which is the typical arrangement for 8-bar columns. All transverse reinforcement was from galvanized iron wires with the nominal diameter of 4.0 mm and the measured yield strength of 353 MPa. The spacing of the hoop set is constant with the value of 43 mm. The volume ratios of the hoop reinforcement are 0.675% and 1.013% for the type *A* confined RAC (A-CRAC) test units and the type *B* confined RAC (B-CRAC) test units, respectively. Two distributions of longitudinal reinforcement were used, and the arrangements consisted of either 4 bars or 8 bars.

The uniaxial deformation of the test unit between the top and the bottom bearing plates was measured via the internal LVDT. In addition, the external axial strain measurement kits with a working range of ±4.00 mm were equipped to measure the local longitudinal strain of RAC in the middle of the test unit corresponding the gauge length of 100 mm.

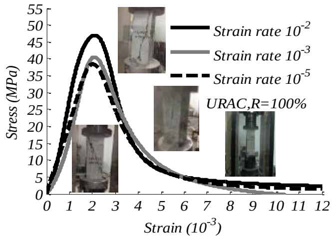

(a) URAC

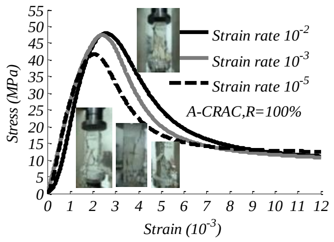

(b) A-CRAC

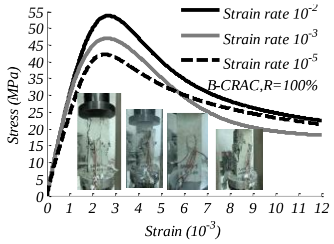

(c) B-CRAC

Fig. 4 Experimental curves of stress-strain

After the preparation of the specimens and the testing machine, the tests were carried out at a series of typically controlled rates of the longitudinal compressive strains of 10^{-5} /s, 10^{-3} /s, and 10^{-2} /s, which correspond to the loading rates of 0.0045 mm/s, 0.45 mm/s, and 4.5 mm/s, respectively.

The typical experimental mean value curves of the total longitudinal stress versus the longitudinal strain for the test units (i.e., URAC A-CRAC, and B-CRAC) under various strain rates are presented in Fig. 4. The mechanical behaviors are calculated from the measured stress-strain curves. The strength and deformation enhancements found in those tests as a result of strain rate effect are consistent with those conclusions by Xiao *et al.* (2005), Zeng *et al.* (2013).

The compressive peak stress increases progressively with the increasing amplitude of loading rates, and the increasing values under the strain rates may be comparable with the results for concrete found by Watstein (1953). The compressive peak strain is defined as the strain when the stress reaches the compressive peak stress. It is implied that in the range of strain rate from 10^{-5}/s to 10^{-2}/s, a significant increase in the compressive peak strain value is observed as the strain rate is increased, although the values of the increase are generally smaller than those observed in compressive peak stress. The changing trend of the compressive peak strain for RAC is consistent with the earlier conclusions by Scott *et al.* (1982), CEB (1993), Bischoff and Perry (1991), and Chen *et al.* (2013).

Table 1 The DIF model parameters

α_a	β_a	θ_a	ϕ	φ
6.664	6.943	8.656	0.01597	0.002

The strain rate effect on the material can be represented by the ratio of the dynamic response to the quasi-static response, well known as the dynamic increase factor (DIF) to describe the rate dependency of the mechanical indices for RAC.

In this study, through regression analysis of experimental data from the dynamic tests, the DIF empirical models expressed as a function of strain rate for the compressive peak stress and the compressive peak strain are developed to depict the enhancement of the compression strength and the critical strain of RAC. The proposed function formulas derived from experimental data are described and expressed in the Eqs. (1) through (2). The relationships described in the following equations are reasonably employed to define the strain-rate dependence of characteristic parameters of recycled aggregate concrete.

$$k_{f_c} = \left(\frac{\dot{\varepsilon}_c}{\dot{\varepsilon}_{c0}} \right)^{\alpha_a \left(\frac{1}{\beta_a + \theta_a f_{cm}} \right)} \tag{1}$$

$$k_{\varepsilon_c} = \left(\frac{\dot{\varepsilon}_c}{\dot{\varepsilon}_{c0}} \right)^{\phi} \tag{2}$$

where k_{f_c} and k_{ε_c} stand for the DIFs of the compressive peak stress, the compressive peak strain, and the compressive ultimate strain of either CRAC or URAC; $\dot{\varepsilon}_c$ denotes the longitudinal compressive strain rate (1/s); $\dot{\varepsilon}_{c0}$ is the longitudinal compressive strain rate at the quasi-static condition, which is referred to as the reference static strain rate parameter and the value is equal to 3.04×10^{-5} /s; f_{cm} is the nominal compressive strength of RAC (MPa), which is equal to 30 MPa according to tests of RAC prism (i.e., 100 *mm* in the side length and 300 mm in the height) under the quasi-static loading condition in this study. The other DIF model parameters are regressed and listed in Table 1.

3. Rate-dependence material model

On the basis of the analysis of the rate-dependence of the mechanical behavior of RAC, the Kent-Scott-Park model (Kent and Park 1971, Scott *et al*. 1982) is adapted for RAC by applying the dynamic increase factors (DIFs) to the compressive peak stress, the compressive peak strain, and the modulus of elasticity, and is illustrated in Fig. 5. The successive degradation of the stiffness of both reloading and the unloading curves is included because of the increasing values in compressive strain, the tension stiffness, and the hysteretic response under seismic conditions (Yassin and Hisham 1994). Thus, the compressive stress-strain relation for CRAC under dynamic monotonic loads can be similarly expressed as

Region OA: $$\sigma_c = K_d f_{cd}' \left[2\left(\frac{\varepsilon_c}{\varepsilon_{do}}\right) - \left(\frac{\varepsilon_c}{\varepsilon_{do}}\right)^2 \right] \quad (\varepsilon_c \le \varepsilon_{d0}) \tag{3}$$

Region AB: $$\sigma_c = K_d f_{cd}' \left[1 - Z_d(\varepsilon_c - \varepsilon_{do})\right] \quad (\varepsilon_{d0} < \varepsilon_c \le \varepsilon_{2d0}) \tag{4}$$

Region BC: $$\sigma_c = 0.2 K_d f_{cd}' \quad (\varepsilon_c > \varepsilon_{2d0}) \tag{5}$$

The corresponding tangent modulus for each region is listed as follows

$$E_c = \frac{2K_d f_{cd}'}{\varepsilon_{do}}\left(1 - \frac{\varepsilon_c}{\varepsilon_{do}}\right) \quad (\varepsilon_c \le \varepsilon_{d0}) \tag{6}$$

$$E_c = -Z_d K_d f_{cd}' \quad (\varepsilon_{d0} < \varepsilon_c \le \varepsilon_{2d0}) \tag{7}$$

$$E_c = 0 \quad (\varepsilon_c > \varepsilon_{2d0}) \tag{8}$$

where

$$f_{cd}' = k_{fc} f_c' \tag{9}$$

$$\varepsilon_{d0} = 0.002 K_d k_{\varepsilon c} \tag{10}$$

$$K_d = \left(1 + \frac{\rho_s f_{yh}}{f_{cd}'}\right) \tag{11}$$

$$Z_d = \frac{0.5}{\dfrac{3 + 0.29 f_{cd}'}{145 f_{cd}' - 1000} + 0.75\rho_s \sqrt{\dfrac{h'}{s_h}} - 0.002 K_d} \tag{12}$$

σ_c and ε_c are the compressive stress and the corresponding strain respectively, ε_{d0} is the compressive critical strain under the dynamic loads, ε_{2d0} is the strain corresponding to 20 % of the compressive peak stress at the descending branch of the stress-strain curve under the dynamic loads, f_c' and f_{cd}' stand for the quasi-static and dynamic axial compressive strength of concrete in *MPa*, respectively, K_d is a factor which accounts for the strength increase due to the confinement and the strain rate effect of concrete, Z_d is the strain softening slope considering the strain rate effect of concrete, f_{yh} is the dynamic yield strength of stirrups in *MPa*, ρ_S is the volume ratio of the hoop reinforcement to the concrete core measured to outside of stirrups, h' is the width of concrete core measured to outside of stirrups, and s_h is the center to center spacing of stirrups or hoop sets. The cyclic unloading and reloading behavior is represented by a set of straight lines as shown in Fig. 5 which shows that hysteretic behavior occurs under both tension and compression stress.

In the model the rate-dependent monotonic tensile stress-strain relation of concrete is described by the following equations

$$\sigma_t = E_t \varepsilon_t \qquad \varepsilon_t < \varepsilon_{td0} \tag{13}$$

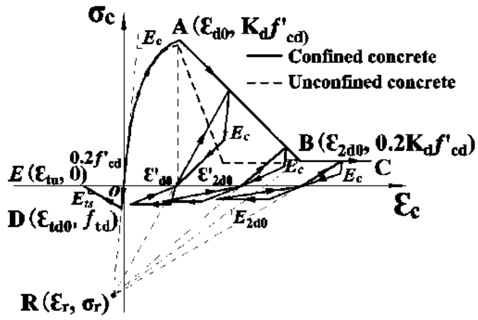

Fig. 5 Modified Kent-Scott-Park model

Table 2 Measured material properties of RAC under the quasi-static loadings

Properties		Compressive strength f_c (MPa)	Elastic modulus E_c (GPa)
Specimens	Floor 1	35.31	24.38
	Floor 2	42.36	26.18
	Floor 3	35.96	24.25
	Floor 4	31.86	23.24
	Floor 5	27.89	21.13
	Floor 6	35.82	23.16

$$\sigma_t = f_{td} + E_{ts}(\varepsilon_t - \varepsilon_{td0}) \qquad \varepsilon_{td0} \le \varepsilon_t < \varepsilon_{tu} \tag{14}$$

with

$$f_{td} = -0.6228\sqrt{k_{ft} f_c'} \tag{15}$$

$$E_t = \frac{f_{td}}{\varepsilon_{td0}} \quad (\varepsilon_t \le \varepsilon_{td0}) \tag{16}$$

where σ_t and ε_t are the tension stress and the corresponding strain respectively, ε_{id0} is the tensile critical strain of concrete, ε_{tu} is the strain at the point where the tensile stress is reduced to zero, which is assumed to be kept unchanged under the dynamic and quasi-static loadings, f_{td} is the tensile strength of concrete under the dynamic condition in MPa, f_c' stands for the quasi-static axial compressive strength of concrete in MPa, E_t is the tensile tangent modulus in the region OD, E_{ts} is the tension stiffening modulus that depends on numerical and physical parameters. The modulus E_{ts} controls the degree of tension stiffening.

According to the results by earlier researchers (Xiao *et al.* 2008, Malvar and Ross 1998), DIF of the tensile peak strain, i.e., the ratio of the tensile peak strain at dynamic loading rate to that at quasi-static loading rate is assumed to be equal to 1.0 in the present work.

In this study, the quasi-static mechanical properties of RAC were measured. Thus, the dynamic stress-strain relation of the modified Kent and Park concrete model can be determined by the above equations, and the tested mechanical properties of RAC under the quasi-static loadings related to the model are listed in Table 2.

4. Modeling of RAC frame structure

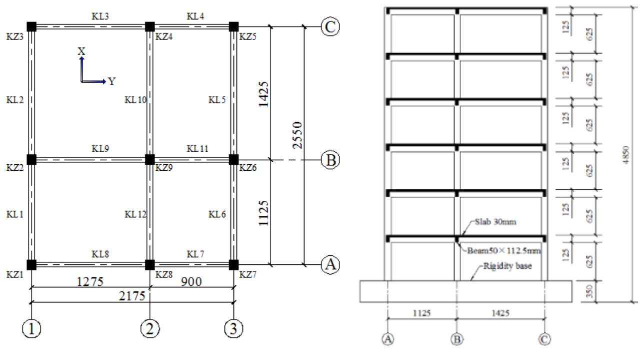

(a) Dimension in plane (b) Dimension in elevation

Fig. 6 Dimension of the six-story frame

Table 3 Similitude scale parameters

Parameter	Model/prototype
Length	1/4
Linear displacement	1/4
Mass	0.034
Damp	0.092
Time	0.368
Rigidity	0.25
Velocity	0.68
Acceleration	1.848
Frequency	2.717

4.1 Shaking table tests

The tested model was a 1/4 scaled two-bay and two-span and six-story frame structure regular in plan and elevation and was designed according to Chinese Building Standard GB 50011 (2010). The RAC frame model was 2175×2550 mm in plan and had a constant story height of 750 mm. The thickness of the slab of the frame model was 30 mm. The details of the general geometry are shown in Fig. 6 (a), (b). The dynamic characteristics of the full-scale structure can be obtained through the similitude relationship of the model and prototype is listed in Table 3.

According to Code for Seismic Design of Buildings (GB 50011 2010), Wenchuan earthquake wave (WCW, 2008, N-S) belonging to Type-II site soil was chosen. Considering the spectral density properties of Type-II site soil, El Centro earthquake wave (ELW, 1940, N-S), Shanghai artificial wave (SHW) were also selected. the earthquake waves were input in the *X* direction of RAC frame structure. The loading program consists of nine phases, that is, tests for peak ground accelerations (PGAs) of 0.066 g, 0.130 g, 0.185 g, 0.264 g, 0.370 g, 0.415 g, 0.550 g, 0.750 g, and 1.170 g.

The typical strain responses for RAC frame structure under earthquake excitations were shown in Fig. 7. The maximum strain is up to about 1854×10^{-6} occurring on the corner column KZ1 in the 0.415 *g* test phase, the strain value is close to the critical strain of RAC, and it is inferred the structure suffers severe damage under the test phase and approaches to the limit state of the maximum bearing capacity.

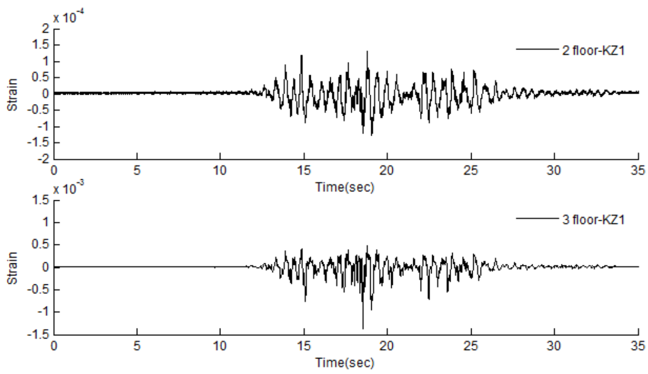

Fig. 7 Strain time history curves under 0.415*g*

Table 4 Maximum strain rate under different test phases (10^{-2}/s)

PGA	Story 2				Story 3		
	Corner column				Corner column		
	KZ3	KZ1	KZ7	KZ5	KZ3	KZ1	KZ7
0.415*g*	0.59	0.56	0.67	1.10	0.76	3.96	4.76
0.550*g*	0.69	4.39	2.07	1.40	0.88	3.51	5.16
0.750*g*	0.71	8.25	3.72	3.40	0.86	5.53	6.91
1.170*g*	1.20	0.65	2.97	3.73	1.57	5.52	9.51
Mean value				3.04			

The strain rate of RAC is calculated by numerical differentiation to the strain response history. The order of magnitude for the maximum strain rates is 10^{-2}/s, which is consistent with the results reported by Bischoff and Perry (1991). In this study, the mean value of 3.04×10^{-2}/s as listed in Table 4 is to be adopted in the material model to perform the dynamic analysis of RAC frame structure.

4.2 Finite element model (FEM)

Based on the OpenSees computational platform, the RAC frame specimen is idealized as a three-dimensional discrete numerical model (shown in Fig. 8), and the frame beam and column members are modeled with the flexibility-based distributed-plasticity nonlinear fiber beam-column elements. For the element, it is subdivided into several control sections and each section is composed of a number of fibers. The number of sections and their locations depends on the integration scheme and the desired level of accuracy. In the numerical implementation of the RAC numerical model, each nonlinear fiber beam-column element is subdivided into five integration points for the numerical simulation performing a good agreement with the experimental results. The number of fibers in a section depends on the geometric and material properties of the section and on the level of detail sought in the section representation. Each fiber is characterized by its area, material type, and position with respect to the section reference system. The origin of the local system is the geometric centroid of the section. The union of the geometric centroids of the section defines the longitudinal axis of the element. Fig. 9(a)-(d) shows the details of the section modeling for the beam and column members, respectively.

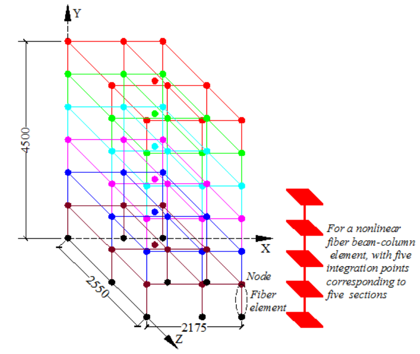

Fig. 8 Numerical model of RAC frame structure

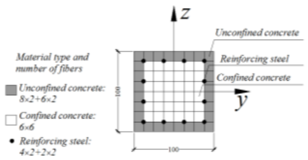

(a) Corner column element section

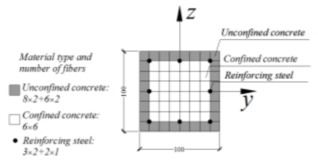

(b) Side and central column element section

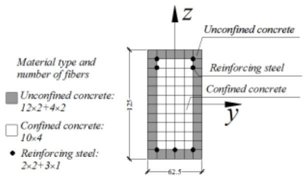

(c) Beam element section in direction Z

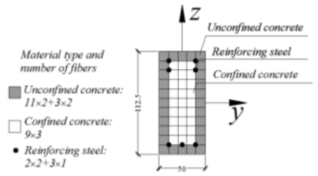

(d) Beam element section in direction X

Fig. 9 Subdivision of cross section into fibers

5. Primary seismic analysis

The typical responses of the structure subjected to WCW, ELW, and SHW excitations and modeled using the material model proposed in the above sections are investigated. The dynamic mechanical behaviors of RAC frame structure obtained from the numerical simulation with exclusion and inclusion of strain rate effect respectively are compared in straight with the shaking table test results. In this section, Model 1 represents the numerical model with the exclusion of strain rate effect, while Model 2 considers the effect of the strain rate of 3.04×10^{-2}/s which is obtained from shaking table tests.

The variation of the lateral stiffness with the excitations of ELW and SHW under different seismic intensity levels is shown in Fig. 10(a)-(b), respectively. The lateral stiffness K_0 under peak ground acceleration (PGA) of 0.130 g is chosen as the reference value in the Figures. The figures show that the lateral stiffness variations for Model 1 and Model 2 agree well with the tested values, more so for Model 2 which considers the strain rate effect than for Model 1 with strain rate excluded. The errors of the lateral stiffness between the numerical and test results increase in the severe elastic-plastic stage. This can be partially attributed to the complex attributes of the materials such as strain softening in compression and tension of recycled aggregate concrete and tensile degradation of reinforcement steel that cannot be captured very well by the analysis procedure in the post-elastic regime.

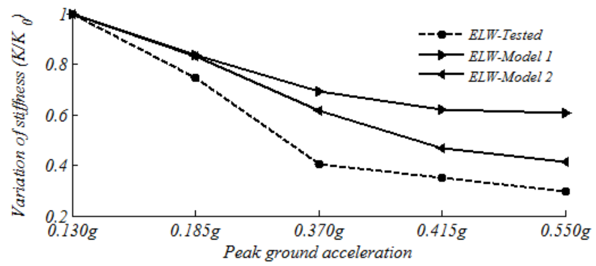

(a) Under ELW excitation history

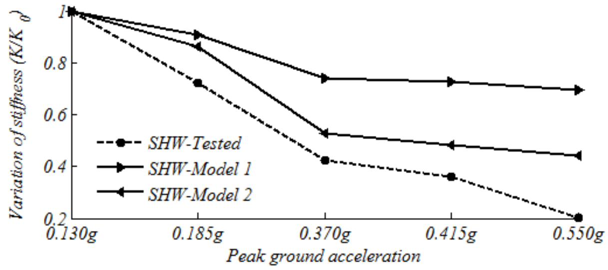

(b) Under SHW excitation history

Fig. 10 Lateral stiffness variation from different excitations

Structures are expected to dissipate energy when subjected to an earthquake ground motion. Part of this energy is dissipated through inelastic elastic-plastic response. As soon as deformations reach the range of inelastic behavior, damage occurs. The hysteresis loop is defined as load-deformation relationship under earthquake loading. It reflects the deformation characteristics, the degradation of strength and stiffness, and the energy dissipation of the structure during the earthquake motions. Some typical hysteresis loops of RAC frame structure subjected to excitation SHW from the numerical simulation are illustrated in Fig. 11 (a)-(c), together with those corresponding to the shaking table test results. Examining the Figures, it can be seen that the hysteretic curve distribution trend for Model 1 or Model 2 is similar to that from shaking table tests, more so for Model 2 than for Model 1. It is again demonstrated the significance of the strain rate effect in the nonlinear dynamic analysis. With the increasing peak ground accelerations (PGAs), the hysteresis loops plump and pinch significantly near the origin of the coordinates. The hysteresis loops show a reversed *S*-shape because of the failure induced by the shear deformation bond slip. With the developing RAC cracks, the lateral stiffness, and the energy dissipation capacity of the structure degrade gradually, and the pinch effect of the hysteresis loops is more obvious. The hysteretic curves under the non-cyclic dynamic loadings behave more disorderly compared with those from the cyclic loading conditions.

6. Secondary seismic analysis

In this study, four different analytical models (NM-1~NM-4) with the strain rates of 3.04×10^{-5} /s, 3.04×10^{-3} /s, 3.04×10^{-2} /s, and 3.04×10^{-1} /s respectively were developed and analyzed, with the same modeling features, analytical procedure, solution algorism, convergence criterion, and dynamic loading input method for the motivation to

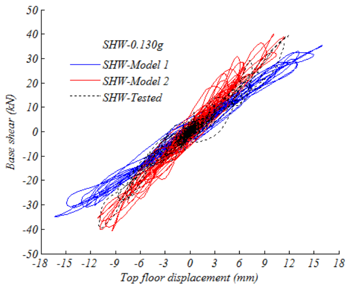

(a) Under 0.130 g

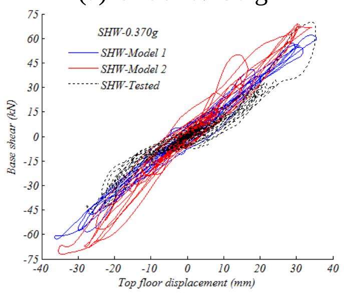

(b) Under 0.370 g

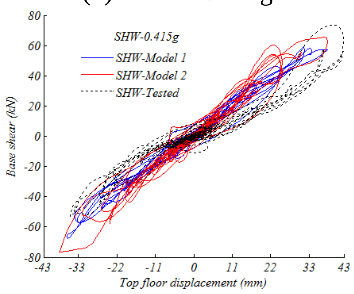

(c) Under 0.415 g

Fig. 11 Comparison of hysteresis loops between the numerical and experimental results

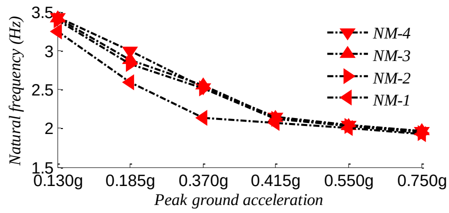

(a) Under WCW

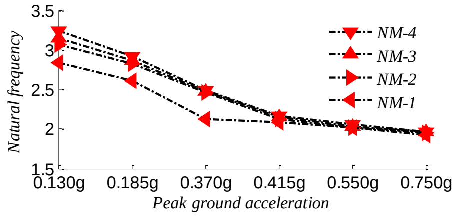

(b) Under ELW

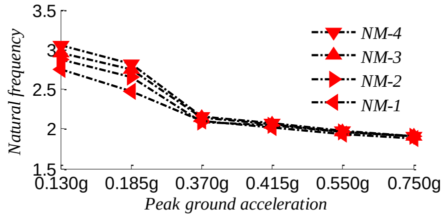

(c) Under SHW

Fig. 12 Natural vibration frequency

Table 5 Parameters of the dynamic lateral stiffness models

Parameter				Curve equation
a_{1i}	b_{1i}	c_{1i}	c_{1i}	
0.106	1.484	0.259	-0.035	K_1
0.509	0.568	0.912	0.057	K_2
1.453	-0.645	1.443	0.121	K_3
3.171	2.788	2.317	0.220	K_4

examine how the dynamic behaviors of RAC frame structure vary under the different strain rates. For comparison, the dynamic responses obtained from the numerical model NM-1 with the strain rate of 3.04×10^{-5} /s are defined as the quasi-static responses.

6.1 Natural vibration frequency

The natural vibration frequencies of RAC frame structure subject to various strain rates are illustrated in Fig. 12 (a)-(c). Comparing the natural frequency variation curves from the four numerical models, it can be seen that the strain rate makes a significant influence on the natural vibration frequency. The natural frequency for NM-1 is larger than for others under the same PGA. On the other hand, the natural frequency for the model NM-4 is the smallest in all numerical models. It is indicated that the natural frequency increases with the increasing strain rates. Under PGAs of 0.066 g to 0.415 g, the strain rate effect makes a significant difference to the natural frequency of the structure. However, the strain rate effect makes a relative little difference to the natural frequency of the structure from 0.415 g to 0.750 g phases.

6.2 Lateral stiffness

The equivalent lateral stiffness K of the structure is estimated with the following expression

$$K = 4M\pi^2 f^2 \tag{17}$$

where, M is the overall mass of RAC frame, and f is the corresponding natural frequency of the structure.

Stiffness degradation occurred when RAC frame structure was subjected to a series of ground motions with an increasing intensity of shaking. Based on the structural lateral stiffness obtained from the four numerical models subjected to WCW, ELW and SHW earthquake history excitations, the model curves for the overall lateral stiffness under the different strain rates are determined and plotted in Fig. 13. The function model derived from the information shown in Fig. 13 for each fitting curve is described as follows

$$K_i(PGA) = \frac{(a_{1i}\cdot PGA^2 + b_{1i}\cdot PGA + c_{1i})}{PGA + d_{1i}} \tag{18}$$

where the PGA is the independent variable in the interval [0.130 g 0.750 g] with g (9.8 N/kg) as the fundamental unit. K_i (i=1, 2, 3, 4) represents the overall dynamic lateral stiffness with the strain rates of 3.04×10^{-1} /s, 3.04×10^{-2} /s,

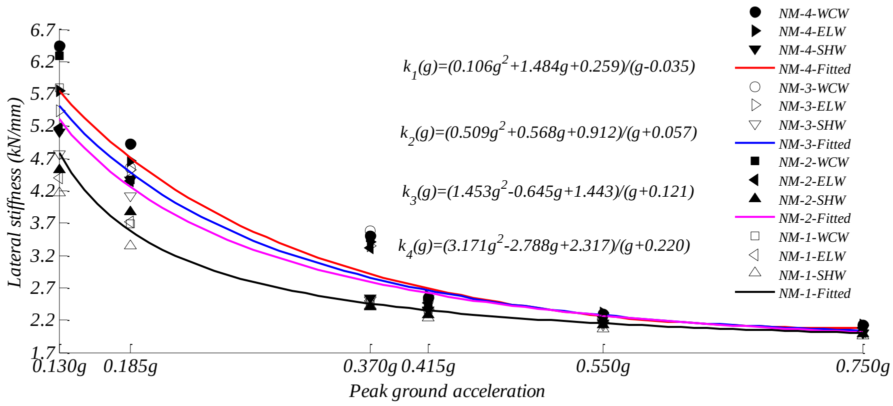

Fig. 13 Dynamic lateral stiffness models

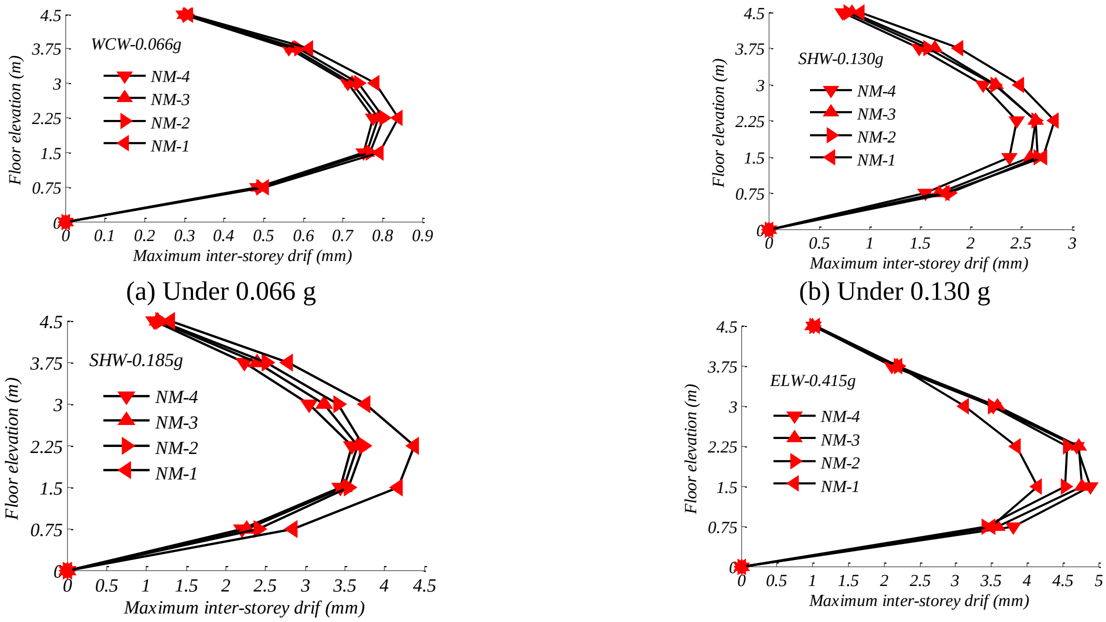

(a) Under 0.066 g (b) Under 0.130 g

(c) Under 0.185 g (d) Under 0.415 g

Fig. 14 Inter-story drift envelopes under different strain rates

3.04×10^{-3} /s, and 3.04×10^{-5} /s, respectively. a_{1i}, b_{1i}, c_{1i} and d_{1i} represent the model parameters, (i=1, 2, 3, 4). The detailed information of the dynamic lateral stiffness model is presented in Table 5.

The relationship described in Eq. (18) is reasonably applied to describe the effect of the strain rate on the lateral stiffness of RAC frame structure. Furthermore, it is simple and reliable to take the stiffness degradation model as the evidence for the accumulated damage degree evaluation of the structure under different earthquake intensity levels.

6.3 Inter-story drift

Inter-story drift is of significant importance to the performance-based seismic design of RAC frame structures because of the good correlation with damage. The story with the maximum inter-story drift could develop into a weak and (or) soft story that initiates the collapse of the structure. The typical inter-story drifts of RAC frame structure subjected to different strain rates are shown in Fig. 14 and listed in Tables 6-8. Comparing the inter-story drifts from the four numerical models, it can be seen the inter-story drifts are significantly different due to the strain rate effect. The inter-story drifts vary significantly in the trend of decreasing with the increasing strain rate under the same earthquake intensity level. Take the phases with PGA of 0.066 g, 0.130 g and 0.185 g for example, the maximum inter-story drifts of RAC frame structure are 3.60 *mm*, 3.66 *mm*, 3.74 *mm*, and 4.37 *mm* for the strain rates of 3.04×10^{-1} /s, 3.04×10^{-2} /s, 3.04×10^{-3} /s, and 3.04×10^{-5} /s, respectively. In addition, under different strain rates, the damage developing for RAC frame structure is also not the same. For the higher strain rate, the damage development stage becomes shorter. Assuming the same damage evolution rate under dynamic loading with different strain rate, the accumulative damage is relatively small for the higher strain rate. Therefore, with the increase of the strain rate, the structural deformation of RAC decreases.

6.4 Base shear coefficient

The base shear coefficient is defined as the ratio of the

Table 6 Maximum inter-story drifts under 0.066 g (mm)

Elevation (mm)	3.04×10^{-1} (1/s)	3.04×10^{-2} (1/s)	3.04×10^{-3} (1/s)	3.04×10^{-5} (1/s)
0.75	0.48	0.49	0.49	0.50
1.50	0.75	0.76	0.77	0.79
2.25	0.78	0.79	0.80	0.84
3.00	0.71	0.72	0.74	0.78
3.75	0.56	0.58	0.59	0.62
4.50	0.30	0.30	0.31	0.31

Table 7 Maximum inter-story drifts under 0.130 g (mm)

Elevation (mm)	3.04×10^{-1} (1/s)	3.04×10^{-2} (1/s)	3.04×10^{-3} (1/s)	3.04×10^{-5} (1/s)
0.75	1.56	1.69	1.75	1.75
1.50	2.38	2.59	2.66	2.71
2.25	2.46	2.64	2.64	2.83
3.00	2.13	2.25	2.24	2.48
3.75	1.49	1.64	1.57	1.88
4.50	0.74	0.82	0.78	0.90

Table 8 Maximum inter-story drifts under 0.185 g (mm)

Elevation (mm)	3.04×10^{-1} (1/s)	3.04×10^{-2} (1/s)	3.04×10^{-3} (1/s)	3.04×10^{-5} (1/s)
0.75	2.21	2.27	2.41	2.85
1.50	3.44	3.48	3.54	4.17
2.25	3.60	3.66	3.74	4.37
3.00	3.05	3.24	3.42	3.76
3.75	2.23	2.40	2.51	2.79
4.50	1.09	1.14	1.17	1.30

total base shear to the total weight of the model. The shear response of RAC frame structure subjected to ground motion excitation is modeled using the numerical models proposed in this study with strain rate effect included. The maximum base shear coefficients with excitation history SHW are plotted in Fig. 15 and listed in Table 9. It is again revealed that the strain rate effect makes a significant difference to the quantity of the base shear coefficient for RAC frame structure. The base shear coefficients at the maximum load points for the models (NM-1 to NM-4) are 0.546, 0.581, 0.601 and 0.622, respectively. It is implied that the base shear coefficient for RAC frame structure increases with the increasing strain rate. Analyzing the base shear vs. PGA curves, it can be revealed that the base shear coefficient increases steeply with the increasing input acceleration amplitudes at the cracking regime with the PGAs from 0.130 g to 0.370 g. The base shear coefficient increases flatly with the increasing input acceleration amplitudes at the yield regime with the PGAs from 0.370 g to 0.550 g, at the yield regime the strain of RAC in compression steps into the hardening stage. For the ultimate regime, with the PGAs from 0.550 g to 0.750 g, the base shear coefficient decreases flatly with the increasing input acceleration amplitudes, then the base shear coefficient decreases steeply up to the PGA of 1.170 g, at the ultimate regime the strain of RAC in comparison steps into softening stage.

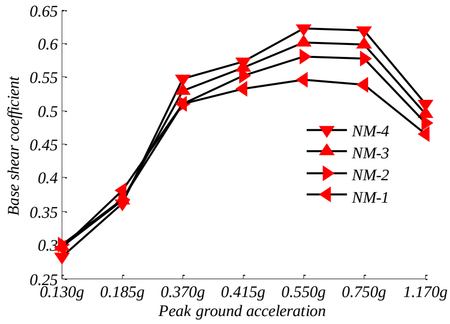

Fig. 15 Base shear coefficient distribution

Table 9 Base shear coefficient of RAC frame structure

PGA	3.04×10^{-1} (1/s)	3.04×10^{-2} (1/s)	3.04×10^{-3} (1/s)	3.04×10^{-5} (1/s)
0.130g	0.282	0.297	0.300	0.296
0.185g	0.362	0.366	0.368	0.381
0.370g	0.547	0.529	0.509	0.510
0.415g	0.574	0.563	0.553	0.533
0.550g	0.622	0.601	0.581	0.546
0.750g	0.620	0.599	0.578	0.539
1.170g	0.511	0.495	0.482	0.466

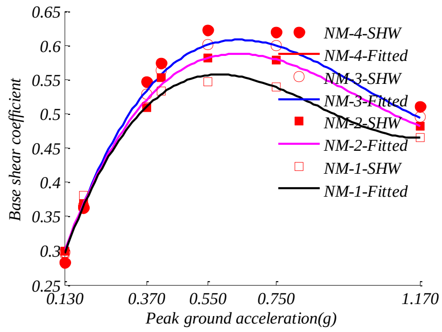

Fig. 16 Model curves for the base shear coefficient

Based on the information presented in Table 9 and Fig. 15, through regression analysis using the MATLAB program, the fitting curves for the base shear coefficient of RAC frame structure subjected to different strain rates are illustrated in Fig. 16. The corresponding function model derived from each fitting curve is expressed as follows

$$BSC_i(PGA) = a_{2i}\cdot(PGA)^3 - b_{2i}\cdot(PGA)^2 + c_{2i}\cdot(PGA) + d_{2i} \quad (19)$$

where *PGA* is defined as the independent variable of the function at the interval [0.130*g* 1.170*g*] with *g* (*9.8 N/kg*) as the fundamental unit. BSC_i (i=1, 2, 3, 4) represents the base shear coefficient with the strain rates of 3.04×10^{-1} /s, 3.04×10^{-2} /s, 3.04×10^{-3} /s, and 3.04×10^{-5} /s, respectively. a_{2i}, b_{2i}, c_{2i} and d_{2i} stand for the function model parameters, (i=1, 2, 3, 4). The fitting function model parameters are presented and listed in Table 10.

When the peak ground acceleration is given, the maximum base shear coefficient can be determined according to the corresponding calculation formula. In addition, it is should be noted that the base shear coefficient model is related to the distribution form of the structural mass.

Table 10 Parameters of the equations for fitting the base shear coefficient

Parameter				Curve equations
a_{2i}	b_{2i}	c_{2i}	d_{2i}	
0.9654	-2.523	1.958	0.082	BS_1
0.7183	-2.127	1.836	0.096	BS_2
0.7582	-2.266	1.971	0.076	BS_3
0.8691	-2.557	2.207	0.036	BS_4

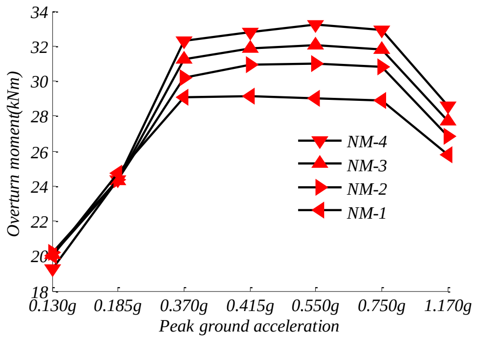

Fig. 17 Base overturning moment distribution

Table 11 Overturn moment of RAC frame structure subjected to different strain rates (kN·m)

PGA	3.04×10^{-1} (1/s)	3.04×10^{-2} (1/s)	3.04×10^{-3} (1/s)	3.04×10^{-5} (1/s)
0.130g	19.258	20.091	20.221	19.989
0.185g	24.372	24.299	24.342	24.753
0.370g	32.324	31.236	30.191	29.047
0.415g	32.816	31.863	30.936	29.136
0.550g	33.229	32.059	30.971	29.022
0.750g	32.892	31.824	30.787	28.894
1.170g	28.553	27.698	26.837	25.754

6.5 Overturning moment

The base overturning moment responses of RAC frame structure subjected to different strain rates under the earthquake excitation SHW are analyzed and illustrated in Fig. 17 and listed in Table 11. The base overturning moments at the maximum load points for the models (NM-1 to NM-4) are 29.022 kN·m, 30.971 kN·m, 32.059 kN·m and 33.229 kN·m, respectively. It is inferred that the base overturning moment for RAC frame structure increases with the increase of the strain rate.

Through the information presented in Fig. 17 and Table 11, based on MATLAB program, the model curves for the base overturning moment of RAC frame structure under dynamic loadings are presented in Fig. 18. The dynamic overturning moment model is expressed in the following form

$$OVM_i(PGA) = a_{3i}\cdot e^{(c_{3i}\cdot PGA)} + b_{3i}\cdot e^{(d_{3i}\cdot PGA)} \qquad (20)$$

where *PGA* is the independent variable in the interval [0.130 g 1.170 g] with g (9.8 N/kg) as the fundamental unit. OVM_i (i=1, 2, 3, 4) stands for the base overturning moment with the strain rates of 3.04×10^{-1} /s, 3.04×10^{-2} /s, 3.04×10^{-3} /s, and 3.04×10^{-5} /s, respectively. a_{3i}, b_{3i}, c_{3i} and d_{3i} represent the dynamic model parameters, (i=1, 2, 3, 4). The results of the fitting are presented in Table 12.

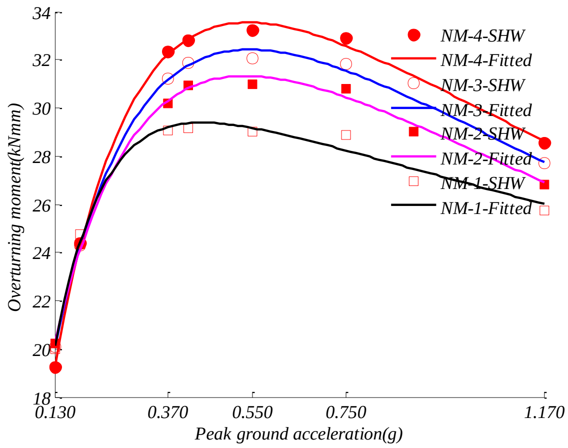

Fig. 18 Model curves of the overturning moment

Table 12 Parameters of the fitting function model for the base overturning moment

Parameter				Curve equations
a_{3i}	b_{3i}	c_{3i}	c_{3i}	
32.80	-39.43	-0.1981	-9.246	OVM_1
40.13	-35.80	-0.3387	-5.257	OVM_2
42.46	-39.59	-0.3602	-5.094	OVM_3
43.31	-45.37	-0.3515	-5.541	OVM_4

The dynamic model for the base overturning moment is important and can be used to evaluate the strength deterioration of RAC frame structure under dynamic loading. Since the damage developing of RAC frame structure under different strain rates behaves significant difference, the accumulative damage is relatively small for the higher strain rate. Therefore, the structural bearing capacity is significantly influenced by the strain rate effect, and the strength of RAC structure increases with the increasing strain rate.

7. Conclusions

Based on the proposed rate-dependent material of RAC, adopting the finite element numerical simulation method, the dynamic mechanical behaviors of RAC frame structure are analyzed and investigated. The main conclusions are described as follows.

- DIF models of the characteristic parameters of RAC are suggested. The dynamic constitutive model of RAC is developed by applying DIFs to the peak stress, the peak strain, and the elastic modulus.
- The lateral stiffness and the hysteresis loops of RAC frame structure obtained from the numerical simulation agree well with the test results, more so for Model 2 which is considered the strain rate effect than for Model 1 with strain rate excluded.
- The natural vibration frequency and the lateral stiffness increase with the increase of the strain rate. The

dynamic model of the lateral stiffness is proposed, which is reasonably applied to describe the effect of the strain rate on the lateral stiffness of RAC frame structure.

• The effect of the strain rate on the structural deformation of RAC is significant. The inter-story drift decreases with the increase of the strain rate.

• The effect of the strain rate on the structural capacity of RAC is analyzed. With the increasing strain rate, the structural capacity increases. The dynamic models of the base shear coefficient and the overturning moment of RAC frame structure are developed. The dynamic models are important and can be used to evaluate the strength deterioration of RAC structure under dynamic loading.

Acknowledgements

The authors wish to acknowledge the financial support from Project funded by China Postdoctoral Science Foundation through Grant Nos. (2014M550247) and (2015T80449), the National Natural Science Foundation of China through Grant No. (51608383), and the Key Projects of Science & Technology Pillar Program of Henan Province (152102310027).

References

ACI Committee 555 (2002), “Removal and reuse of hardened concrete”, *ACI Mater. J.*, **99**(3), 300-325.

Ajdukiewicz, A.B. and Kliszczewicz, A.T. (2007), “Comparative tests of beams and columns made of recycled aggregate concrete and natural aggregate concrete”, *J. Adv. Concrete Technol.*, **5**(2), 259-73.

Ashtiani, R., Saeed, A. and Hammons, M. (2014), Mechanistic characterization and performance evaluation of recycled aggregate systems”, *J. Mater. Civil Eng.*, **26**(1), 99-106.

Behera, M., Bhattacharyya, S.K., Minocha, A.K., Deoliya, R. and Maiti, S. (2014), “Recycled aggregate from C&D waste & its use in concrete-A breakthrough towards sustainability in construction sector: A review”, *Constr. Build. Mater.*, **68**, 501-516.

Bischoff, P.H. and Perry, S.H. (1991), “Compressive behavior of concrete at high strain rates”, *Mater. Struct.*, **24**(6), 425-450.

Cardoso, R., Silva, R.V., de Brito, J. and Dhir, R. (2016), “Use of recycled aggregates from construction and demolition waste in geotechnical applications: A literature review”, *Waste Manage.*, **49**, 131-145.

Chen, X.D., Wu, S.X. and Zhou, J.K. (2013), “Experimental and modeling study of dynamic mechanical properties of cement paste, mortar and concrete”, *Constr. Build. Mater.*, **47**, 419-430.

Fathifazl, G., Razaqpur, A.G., Isgor, O.B., Abbas, A., Fournier, B. and Foo, S. (2009), “Flexural performance of steel-reinforced recycled concrete beams”, *ACI Struct. J.*, **106**(6), 858-67.

GB 50011 (2010), Code for Seismic Design of Buildings, Chinese Building Press, Beijing, China.

Gnjatovic, I.S., Marinkovic, S.B., Miskovic, Z.M. and Savic, A.R. (2013),”Flexural behavior of reinforced recycled aggregate concrete beams under short-term loading”, *Mater. Struct.*, **46**(6), 1045-1059.

Kent, D.C. and Park, R. (1971), “Flexural members with confined concrete”, *J. Struct. Div.*, ASCE, **97**(ST7), 1969-1990.

Kwak, H.G., Kim, S.P. and Kim, J.E. (2004), “Nonlinear dynamic analysis of RC frames using cyclic moment-curvature relation”, *Struct. Eng. Mech.*, **17**(3-4), 357-378.

Lotfi, S., Eggimann, M., Wagner, E., Mroz, R. and Deja, J. (2015), “Performance of recycled aggregate concrete based on a new concrete recycling technology”, *Constr. Build. Mater.*, **95**, 243-256.

Lu, Y. and Tu, Z.G. (2011), “Mesoscale modelling of concrete for static and dynamic response analysis Part 2: numerical investigations”, *Struct. Eng. Mech.*, **37**(2), 215-231.

Lu, Y.B., Chen, X., Teng, X. and Zhang S. (2014), “Dynamic compressive behavior of recycled aggregate concrete based on split Hopkinson pressure bar tests”, *Latin Am. J. Solid. Struct.*, **11**(1), 131-141.

Malvar, L.J. and Ross, C.A. (1998), “Review of strain rate effects for concrete in tension”, *ACI Mater. J.*, **95**(6), 735-739.

Penelis, G.G. and Kappos, A.J. (1997), *Earthquake-resistant Concrete Ctructures*, E & FN Spon.

Rahal, K.N. and AI-Khaleefi, A.L. (2015), “Shear-friction behavior of recycled and natural aggregate concrete-an experimental investigation”, *ACI Struct. J.*, **112**(6), 725-733.

Scott, B.D., Park, R. and Priestley, M.J.N. (1982), “Stress-strain behavior of concrete confined by overlapping hoops at low and high strain rates”, *ACI J.*, **79**(1), 13-27.

Shao, Y., Aval, S. and Mirmiran, A. (2005), “Fiber-element model for cyclic analysis of concrete-filled fiber reinforced polymer tubes”, *J. Struct. Eng.*, ASCE, **131**(2), 292-303.

Shi, X.S., Wang, Q.Y., Zhao, X.L. and Collins, F.G. (2015), ”Structural behaviour of geopolymeric recycled concrete filled steel tubular columns under axial loading”, *Constr. Build. Mater.*, **81**, 187-197.

Shing, P.S.B. and Mahin, S.A. (1988), “Rate of loading effects on pseudo dynamic tests”, *J. Struct. Eng.*, ASCE, **114**(11), 2403-2420.

Taucer, F.F., Spacone, E. and Filippou, F.C. (1991), “A fiber beam-column element for seismic response analysis of reinforced concrete structures”, Report No. UCB/EERC-91/17; Earthquake Engineering Research Center, University of California, Berkeley.

The Euro-International Committee for Concrete (CEB) (1993), CEB-FIP Model Code 1990, Lausanne, Switzerland, Thomas Telford Ltd.

Tu, Z.G. and Lu, Y. (2011), “Mesoscale modelling of concrete for static and dynamic response analysis Part 1: model development and implementation”, *Struct. Eng. Mech.*, **37**(2), 197-213.

Valipour, H.R. and Foster, S.J. (2010), “Nonlinear analysis of 3D reinforced concrete frames: effect of section torsion on the global response”, *Struct. Eng. Mech.*, **36**(4), 421-444.

Wakabayashi, M., Nakamura, T., Iwai, S. and Hayashi, Y. (1984), “Effect of strain rate on the behavior of structural members subjected to earthquake force”, *Proceeding 8th World Conference on Earthquake Engineer*, San Francisco, USA.

Wang, C.Q. (2012), “Study on shaking table tests and nonlinear seismic response analysis of recycled aggregate concrete frame structure”, Ph.D. Dissertation, Tongji University, Shanghai, China.

Wang, C.Q. and Xiao, J.Z. (2012a), “Shaking table tests on a recycled concrete block masonry building”, *Adv. Struct. Eng.*, **15**(10), 1843-1860.

Wang, W.J., Zhao, L., Liu, Y.Z., Li, Z. (2014), “Mechanical properties and stress-strain relationship in axial compression for concrete with added glazed hollow beads and construction waste”, *Constr. Build. Mater.*, **71**, 425-434.

Watstein, D. (1953), “Effect of straining rate on the compressive strength and elastic properties of concrete”, *ACI J., Pr.*, **49**(8), 729-744.

Xiao, J.Z., Li, J.B. and Zhang, C.H. (2005), “Mechanical properties of recycled aggregate concrete under uniaxial loading", *Cement Concrete Res.*, **35**, 1187-1194.

Xiao, J.Z., Li, L., Shen, L.M. and Poon, C.S. (2015), "Compressive behaviour of recycled aggregate concrete under impact loading", *Cement Concrete Res.*, **71**, 46-55.

Xiao, J.Z., Yuan, J.Q. and Li, L. (2014), "Experimental study on dynamic mechanical behavior of modeled recycled aggregated concrete under uniaxial compression", *J. Build. Struct.*, **35**(3), 26-207.

Xiao, S., Li, H. and Lin, G. (2008), "Dynamic behaviour and constitutive model of concrete at different strain rates", *Mag. Concrete Res.*, **60**(4), 271-278.

Zeris, C.A. and Mahin, S.A. (1991), "Behavior of reinforced concrete structures subjected to biaxial excitation", *J. Struct. Eng.*, ASCE, **117**(9), 2657-2673.

Zhang, J.W., Cao, W.L., Meng, S.B., Yu, C. and Dong, H.Y. (2014), "Shaking table experimental study of recycled concrete frame-shear wall structures", *Earthq. Eng. Eng. Vib.*, **13**(2), 257-267.

Zhang, J.W., Dong, H.Y., Cao, W.L., Yu, C. and Chi, Y.Z. (2016), "Shaking table tests of low-rise shear walls made of recycled aggregate concrete", *Struct. Eng. Int.*, **26**(1), 62-73.

Zhang, S. and Zong, L. (2014), "Properties of concrete made with recycled coarse aggregate from waste brick", *Environ. Pr. Sustain. Energy*, **33**(4), 1283-1289.

Zhao, J.L., Yu, T. and Teng, J. (2015), "Stress-strain behavior of FRP-confined recycled aggregate concrete", *J. Compos. Construct.*, **19**(3), 04014054-1-11.

PL